DOI: 10.1002/anie.201304496

Porous Polymer Sandwiches

Two-Dimensional Sandwich-Type, Graphene-Based Conjugated Microporous Polymers**

Xiaodong Zhuang, Fan Zhang, Dongqing Wu, Nina Forler, Haiwei Liang, Manfred Wagner, Dominik Gehrig, Michael Ryan Hansen, Frédéric Laquai, and Xinliang Feng**

Porous polymers[1] with porosity at the nanoscale have attracted tremendous attention since their porous features are associated with prominent physical properties and since they have potential applications in, for example, light harvesting,[2] sensing,[3] gas separation[4] and storage,[5] catalysis,[6] and energy storage and conversion.[7] There are several classes of micro-/mesoporous polymers, such as hyper-crosslinked polymers (HCPs), polymers of intrinsic microporosity (PIMs), and covalent organic frameworks (COFs). Porous polymers can be also classified according to their structural conformations as amorphous- (HCPs and PIMs) or crystalline-type (COFs) materials.[1e] Conjugated microporous polymers (CMPs) represent one of the fastest developing types of porous materials not only because of their efficient synthesis by conventional metal-catalyzed polymerization techniques and the availability of a large number of commercially available functional monomers but also due to their controllable and adaptable physical properties.[1d] Unlike COFs, CMPs are formed under kinetic control, and thus are amorphous and show no long-range structural order.[8] For this reason, most of the previous work on CMPs has been focused on developing new chemical strategies and tuning the pore size distribution and surface area of these polymers by varying the length of the organic linkers rather than through morphology control. Very recently, efforts have been made to synthesize CMPs with controlled nanostructures, such as quasi-zero-dimensional microspheres,[9] and one-dimensional nanofibers[10] and nanotubes[11] as well as three-dimensional monoliths.[12] However, the synthesis of porous polymers with two-dimensional (2D) sheet structures remains little explored. Dichtel et al. employed a solvothermal method to grow oriented 2D COF thin films on substrate-supported graphene by the dynamic assembly of boronic acid and hexahydroxytriphenylene monomers,[13] but the large-scale production of free-standing 2D porous polymer networks has not yet been achieved.

Graphene, because of its single-atom thickness, large aspect ratio, high surface area, and many intriguing physical properties, has proved to be a promising template for the highly efficient construction of 2D porous nanohybrid materials, such as 2D porous silica,[14] metal oxides,[15] metal sulfides,[16] carbon nitride,[17] and carbon-coated graphene/metal oxide sheets.[18] All these approaches typically rely on the use of a graphene-based porous silica template in nanocasting technology or the nucleation of metal oxide or sulfide nanostructures on the graphene surface. Nevertheless, the porous structures of these graphene-based hybrid materials cannot be tailored at the molecular level, as has been done for organic porous materials.[1]

We report herein on a graphene-inspired synthetic approach to the large-scale production of 2D sandwichlike conjugated microporous polymers in which each graphene sheet is fully separated by a porous polymer shell. Thiophene-, thiazole-, and pyridine-based monomers can be polymerized with 1,3,5-triethynylbenzene monomer on the graphene surface through the metal-catalyzed Sonogashira–Hagihara coupling reaction. The resulting porous polymer nanosheets exhibit large aspect ratios, high surface areas, and fluorescence quenching. These unique structural features associated with a graphene sheet confined within a polymer network establish a new generation of porous materials with multiple functions.

The strategy for the synthesis of 2D graphene-based conjugated microporous polymer sheets (GMPs) is presented in Scheme 1. First, a graphene oxide sheet (GO) was reduced with hydrazine hydrate (→RGO)[19] and then functionalized by treatment with a *p*-bromobenzene diazonium salt under aqueous conditions. The obtained bromo-functionalized RGO (RGBr) was highly dispersed in various organic solvents, such as dimethylformamide (DMF, 1.0 mg mL^{-1}; see Figure S1 in the Supporting Information), chloroform, and toluene. Next, halogenated thiophene-, thiazole-, and pyridine-based monomers (M^2) were mixed with 1,3,5-triethynylbenzene (M^1) and RGBr in anhydrous DMF along with [Pd(PPh$_3$)$_4$] and CuI, and the reaction mixture was sealed and stirred under Sonogashira–Hagihara reaction conditions. After precipitation, a black solid was collected and purified by Soxhlet extraction. Finally, 2D sandwichlike GMPs, denoted as GMP-S, GMP-NS, and GMP-N for the thiophene-, thiazole-, and pyridine-containing polymers, respectively,

[*] Dr. X. D. Zhuang, Prof. F. Zhang, Prof. D. Wu, Prof. X. Feng
College of Chemistry and Chemical Engineering
Shanghai Jiao Tong University
800 Dongchuan Road, Shanghai 200240 (P. R. China)
E-mail: fan-zhang@sjtu.edu.cn
feng@mpip-mainz.mpg.de
Dr. N. Forler, Dr. H. Liang, Dr. M. Wagner, Dr. D. Gehrig, Dr. M. R. Hansen, Dr. F. Laquai, Prof. X. Feng
Max Planck Institute for Polymer Research
Ackermannweg 10, 55128 Mainz (Germany)

[**] This work was financially supported by the National Basic Research Program of China (973 Program: 2012CB933404), the Natural Science Foundation of China (21174083 and 21102091), BASF, the Shanghai Pujiang Program (11J1405400), the PhD Programs Foundation of the Ministry of Education of the People's Republic China for Young Scholars (20110073120039), and an ERC grant on 2DMATER.

Supporting information for this article is available on the WWW under http://dx.doi.org/10.1002/anie.201304496.

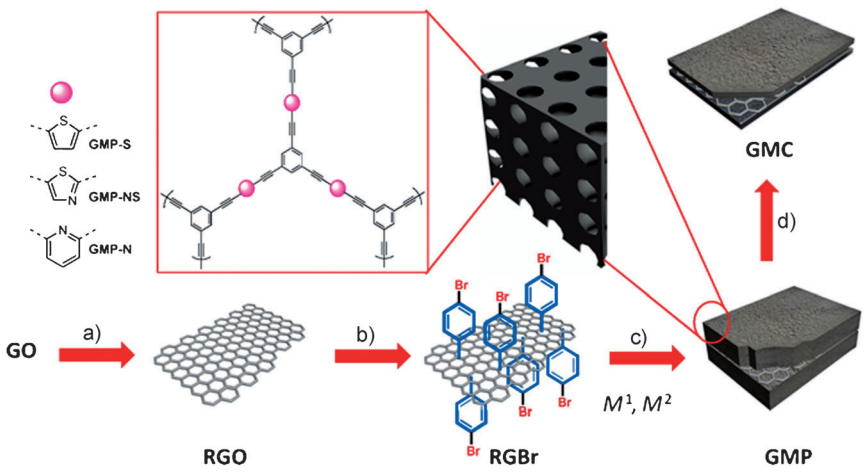

Scheme 1. Preparation of GMPs and related graphene-based microporous carbons (GMCs). a) Sodium dodecylbenzenesulfonate, $N_2H_4{\cdot}H_2O$, 100 °C, 8 h; b) 4-bromobenzenediazonium tetrafluoroborate, 0 °C to RT, 2 h; c) Ar, $[Pd(PPh_3)_4]$, CuI, Et_3N, DMF, 80 °C, 3 days (M^1 = 1,3,5-triethynylbenzene; M^2 = 2,5-dibromothiophene, 2,5-dibromo-1,3-thiazole, and 2,6-dibromopyridine); d) Ar, RT to 800 °C, 5 °C min^{-1}, 2 h.

were obtained after vacuum drying. The use of highly dispersible RGBr in our approach not only effectively solves the incompatibility and aggregation problems between the graphene layers and the porous polymers but also provides the 2D template for the efficient growth of porous polymers on the graphene surface. The microporous polymers (MPs) were also prepared without the graphene template for comparison in this work, and are denoted as MP-S, MP-NS, and MP-N, respectively (Scheme S1 in the Supporting Information).

The morphology and microstructure of the as-prepared GMPs were investigated by scanning electron microscopy (SEM), transmission electron microscopy (TEM), and atomic force microscopy (AFM). All of the GMPs showed similar sheet morphology. Thus, the results of GMP-S are discussed here as a typical example. As shown in Figure 1 a–c and Figure S3, many free-standing sheets with morphology similar to that of graphene and with sizes ranging from 200 nm to several micrometers were observed. In addition, these porous polymer sheets exhibited wrinkles and flexible features that stand in contrast to the rigid inorganic porous silica sheets[14a] reported previously. No free porous polymer particles or naked graphene sheets were seen in either the TEM or SEM images. This suggests that, as expected, most of the monomers have been polymerized on the surface of graphene (Figure S2).[20] Typical AFM and thickness analyses (Figure 1 b) revealed the same morphology as that observed with SEM and TEM, with a uniform thickness of (40 ± 3) nm. The control sample MP-S without the graphene template exhibited the same amorphous nanoparticle structure (Figure S3a) as that previously reported.[21] These results strongly suggest the crucial role of graphene as a substrate for the grafting of conjugated microporous polymers in a 2D manner.

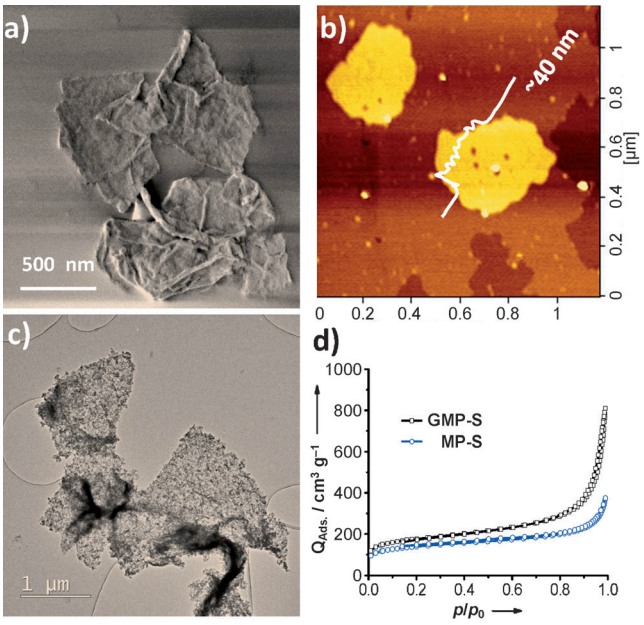

Figure 1. Graphene-based 2D conjugated microporous polymers. Typical a) SEM, b) AFM, and c) TEM images of GMP-S. d) Nitrogen adsorption/desorption isotherms of MP-S and GMP-S.

Initially, we were concerned that the involvement of graphene in the synthesis would reduce the degree of polymerization and expose large numbers of end groups, owing to the micrometer scale of the length/width of the graphene sheets, and thus affect the porosity of the resulting materials. To analyze the molecular structure of GMP-S, solid-state ^{13}C NMR spectroscopy was employed (Figure 2 a). These spectra were recorded using $^{13}C\{^1H\}$ cross-polarization magic-angle-spinning (CP/MAS) NMR spectroscopy with different CP times.[22] This enabled us to distinguish between ^{13}C atoms with directly attached protons (short CP time) and quaternary ^{13}C atoms (longer CP time).[23] Thus, from a comparison of the two $^{13}C\{^1H\}$ CP/MAS NMR spectra in Figure 2 a, the resonances at 83.4 and 93.1 ppm can be assigned to the -C≡C- linkages, whereas the ^{13}C resonances of the proton-bearing atoms located at 124.3, 127.8, and 131.4 ppm are assigned to the thiophene and phenylene groups.[8,24] No evidence of -C≡C-H end groups could be seen, since these would give rise to signals in the region from 80.0 to 100.0 ppm in spectrum (1) in Figure 2 a. Further details on the assignment can be found in Figures S5 and S6 in the Supporting Information.

Given the conjugated nature of the polymer networks, we further investigated the exciton dynamics of GMP-S and MP-S by time-resolved photoluminescence spectroscopy. As shown in Figure 2 b and Figure S7, MP-S exhibits a stretched exponential decay indicating a distribution of lifetimes. The decay can be fit with an inverse rate constant of 5.19 ps and a stretching exponent of 0.34. The stretching exponent (β = 0.31) is found to be similar to that of GMP-S, while the decay

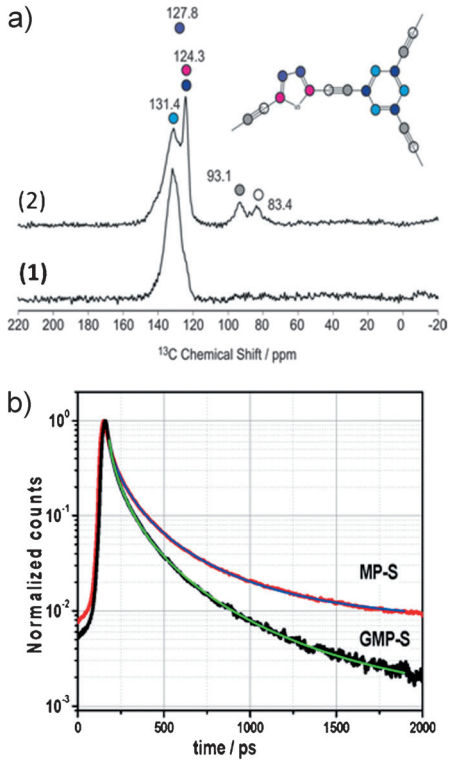

Figure 2. a) Solid-state $^{13}C\{^{1}H\}$ CP/MAS NMR spectra of GMP-S recorded using CP contact times of 0.2 ms (spectrum (1)) and 3.0 ms (spectrum (2)). All spectra were recorded at a static magnetic field of 16.4 T using a MAS frequency of 25.0 kHz. The inset illustrates the assignment scheme. b) Fluorescence decay of MP-S (red) and GMP-S (black) monitored at $\lambda = 550$–600 nm and the respective stretched exponential fits ($\lambda_{ex} = 400$ nm).

is significantly faster with an inverse rate constant of 1.76 ps. This result implies that an electronic interaction exists between the graphene sheet and the porous polymer network in GMP-S, whose nature is the subject of further investigation. However, it appears that the graphene sheet acts as an electron acceptor, while the conjugated microporous polymer shell serves as an electron donor. Such a sandwichlike D–A–D-type porous organic material, in which graphene sheets act as an ultrathin electron-accepting layer, may hold promise for certain electronic applications.

The porous nature of the GMPs was confirmed by nitrogen physisorption measurements. It was found that the isotherms of both GMP-S and MP-S are type I (Figure 1d) and the others are type IV (Figure S8). The Brunauer–Emmet–Teller (BET) surface areas of these polymer networks varied between 458 and 888 $m^2 g^{-1}$ (Table S1). Typically, the specific surface area of MP-S was 689 $m^2 g^{-1}$, which is within the range of 262–880 $m^2 g^{-1}$ reported for similar MPs.[8] In contrast, GMP-S yielded a BET surface area as high as 888 $m^2 g^{-1}$. The micropore size distribution of GMP-S and MP-S is presented in Figure S9. GMP-NS and GMP-N show similar results which indicate that the high surface area of MPs can be achieved by taking advantage of the 2D structure of graphene sheets.

Conjugated microporous polymers can serve as a type of carbon-rich precursor[25] that can integrate heteroatoms,[26] metals, and metal oxides[11] into the carbon framework for various applications, such as energy storage and electrochemical catalysis. Thermogravimetric analysis (TGA) revealed that both MPs and GMPs can feasibly be transformed into carbon materials with a high carbon yield (70–90%, Figure S10). Therefore, S-, N/S-, and N-doped 2D porous carbons, denoted as GMC-S, GMC-NS and GMC-N, respectively, were generated by the direct pyrolysis of GMPs at 800 °C for 2 h under an argon atmosphere (Scheme 1). The TEM images in Figure 3a and nitrogen physisorption results (Table S1) indicate that GMC-S, GMC-NS, and GMC-N maintain the 2D morphology of the microporous polymers with a large aspect ratio as well as the porosity with a high BET surface area of 618, 681, and 560 $m^2 g^{-1}$, respectively. As far as we know, this is the first example of the preparation of 2D porous carbon nanosheets without the use of any inorganic porous templates. For comparison, porous carbons were also prepared by the same procedure from MPs but without a graphene template, and are denoted as MC-S, MC-NS, and MC-N, respectively: their surface areas were in the range 554–636 $m^2 g^{-1}$. The decrease in the surface area for the GMCs and MCs with respect to the corresponding GMPs and MPs is probably due to the degradation of polymers and recombination of fragments under the carbonization conditions.[25]

The chemical nature of the GMCs was further investigated by X-ray photoelectron spectroscopy (XPS) and elemental analysis. Interestingly, the S 2p spectra of both GMC-S and GMC-NS can be fitted by the same sulfur components,[27] while the N 1s spectra of GMC-NS and GMC-N correspond to almost the same fitted nitrogen components (Figures S11–S13). The weight content of sulfur in GMC-S and GMC-NS was 7.7% and 5.9%, respectively, and the nitrogen content in GMC-NS and GMC-N reached 3.0% and 3.8%, respectively. This strategy thus provides a feasible way to build up 2D porous carbons with a high level of heteroatom doping (Table S2).

One of the most important applications of heteroatom-doped porous carbons is as metal-free catalysts for the oxygen reduction reaction (ORR). N/S co-doped carbon materials[28] have been demonstrated to exhibit better electrocatalytic performance than singly N- or S-doped carbon materials. We examined the electrocatalytic activities of our N- and/or S-doped 2D porous carbons towards the ORR under alkaline conditions (0.1 M KOH). The ORR catalytic activity of the GMCs was first evaluated by cyclic voltammetry (CV, Figure 3c). GMC-S showed an ORR onset potential of −0.15 V and a peak potential of −0.28 V versus Ag/AgCl, values that were slightly lower than the results for GMC-NS and GMC-N. The Koutecky–Levich plots (K-L plots; inset in Figure 3d) with a good linear relationship for the GMC-S electrode were calculated from linear sweep voltammetry (LSV) curves (Figure S14) at various rotation rates. Notably, the mean number of transferred electrons (n) per O_2 molecule involved in the ORR, which can be determined from the K-L equation [Eq. (S1)], was approximately 4.0 between −0.45 V and −0.90 V. A similar value for n (ca. 3.90 at −0.50 V) can be calculated from the rotating ring-disk electrode (RRDE) curve [Figure 3d and Eq. (S3)]. These results highlight that

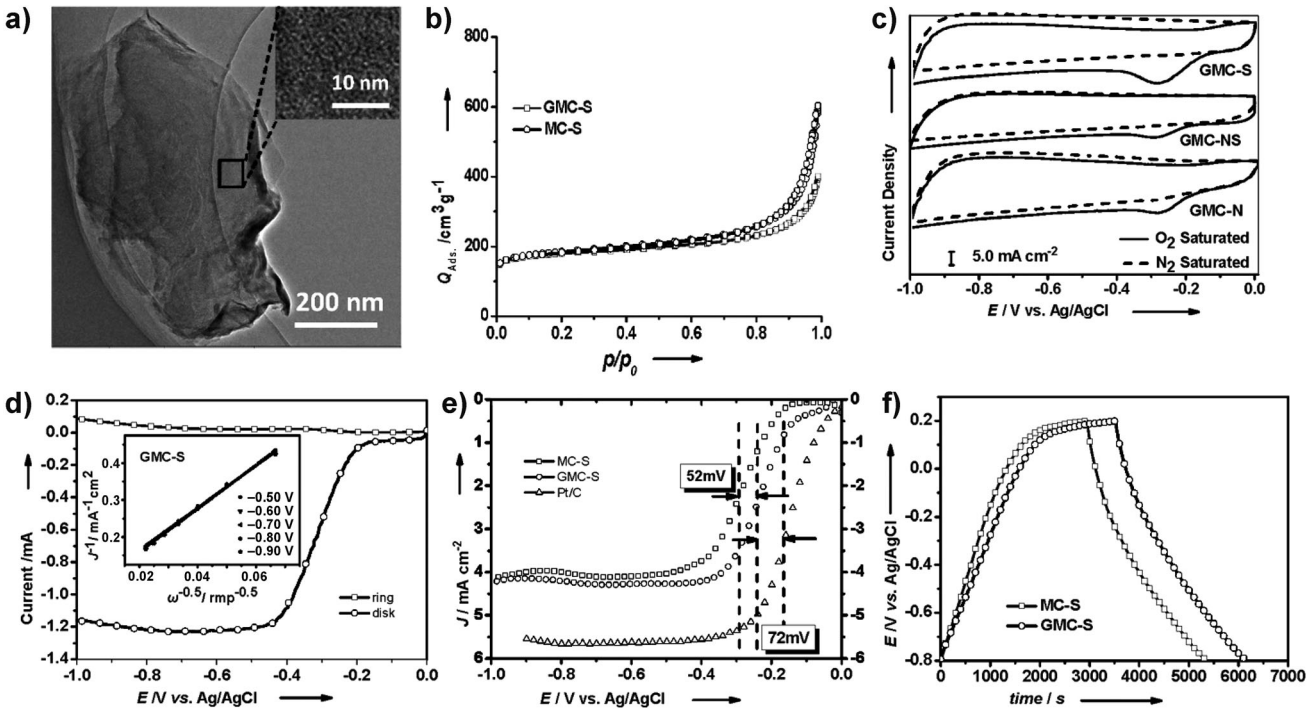

Figure 3. Graphene-based 2D porous carbons (GMCs) and their ORR and supercapacitor performances. a) TEM image of GMC-S; b) nitrogen adsorption/desorption isotherms of MC-S and GMC-S disclosing their 2D shape and porous nature; c) CV curves of GMCs in N_2-saturated (dashed line) and O_2-saturated (solid line) 0.1 M KOH at a scan rate of 50 mV s^{-1}; d) RRDE curve of GMC-S at 1600 rpm (the inset shows Koutecky–Levich plots derived from the RDE measurement); e) LSV curves of MC-S, GMC-S, and Pt/C in O_2-saturated 0.1 M KOH solution at 1600 rpm at a scan rate of 5 mV s^{-1}; f) galvanostatic charge/discharge curves of MC-S and GMC-S at a current density of 0.1 A g^{-1}.

the ORR proceeds by a primarily four-electron pathway.[29] Figure 3e shows the corresponding LSV curves for MC-S, GMC-S, and Pt/C in an O_2-saturated 0.1M KOH electrolyte. Of note, the half-wave potential (HWP) for the ORR with GMC-S occurred at −0.23 V, which is 52 mV lower than that with MC-S. Further, GMC-NS and GMC-N exhibited a similar decrease in HWP values (Figures S15–S17) in comparison with those of MC-NS (by 97 mV) and MC-N (by 90 mV), suggesting a lower operation voltage and lower energy consumption for GMCs. Although the diffusion-limiting current densities ($J_{DL} \approx 4.0$ mA cm^{-2}) of the GMCs catalysts were lower than that of commercial Pt/C (BASF, ca. 5.5 mA cm^{-2}), the mainly four-electron-transfer pathway (peroxide yield of about 5% at −0.50 V), together with the very low HWP potential, make GMCs still promising as metal-free electrocatalysts for ORR. The kinetic-limiting current of GMC-S was calculated [Eq. (S1)] to be 27.0 mA cm^{-2}, which is higher than those of GMC-NS (13.5 mA cm^{-2}) and GMC-N (10.8 mA cm^{-2}), and also much higher than that of most reported Pt/C catalysts.[29]

In addition to their excellent ORR performance, GMCs also exhibited outstanding supercapacitive behavior. The capacitive performance was investigated through galvanostatic charge/discharge cycling experiments (Figure 3f and Figure S20). On the basis of the discharging curve line, the specific gravimetric capacitance of GMCs was calculated to be 244–304 F g^{-1} at 0.1 A g^{-1}, which is 14–35% higher than that of MCs. The further calculated specific capacitances per surface area (C_{SA}) of GMCs are all almost uniformly 12–13% higher than those of MCs. Moreover, the C_{SA} of GMCs and MCs was found to be superior to that reported for RGO[30a] and KOH-activated graphene,[30b] and comparable to that of 3D porous carbon[30c] and B/N co-doped graphene aerogel[30d] (Table S3). For both the ORR and supercapacitor applications, the graphene layer in the sandwich-type GMCs is expected to act as a miniature current collector and a long-distance in-plane charge transporter during the electrochemical processes, by taking advantage of its high electrical conductivity and 2D electron transport feature.

In summary, we have demonstrated a novel graphene-inspired strategy for the synthesis of 2D conjugated microporous polymers with large aspect ratios and high specific surface areas. These 2D porous polymers were used to prepare heteroatom-doped 2D porous carbons by thermal carbonization without a template. The resulting S- and N-doped 2D porous carbon materials exhibited high efficiency as metal-free catalysts for ORR, associated with prominent supercapacitive behavior. It is expected that our synthetic strategy will offer the opportunity to build up various 2D porous polymers and carbons that provide an important platform for developing a variety of functional devices, such as batteries, fuel cells, electronics, and sensors.

Received: May 24, 2013
Published online: July 24, 2013

Keywords: conjugated microporous polymers · donor–acceptor systems · graphene · oxygen reduction reaction · porous carbon

[1] Recent publications: a) D. Wu, F. Xu, B. Sun, R. Fu, H. He, K. Matyjaszewski, *Chem. Rev.* **2012**, *112*, 3959 – 4015; b) M. S. Silverstein, N. R. Cameron, M. A. Hillmyer, *Porous Polymers*, Wiley, Hoboken, **2011**; c) R. Dawson, A. I. Cooper, D. J. Adams, *Prog. Polym. Sci.* **2012**, *37*, 530 – 563; d) A. Thomas, *Angew. Chem.* **2010**, *122*, 8506 – 8523; *Angew. Chem. Int. Ed.* **2010**, *49*, 8328 – 8344; e) J. W. Colson, W. R. Dichtel, *Nat. Chem.* **2013**, DOI: 10.1038/nchem.1628.

[2] L. Chen, Y. Honsho, S. Seki, D. L. Jiang, *J. Am. Chem. Soc.* **2010**, *132*, 6742 – 6748.

[3] X. M. Liu, Y. H. Xu, D. L. Jiang, *J. Am. Chem. Soc.* **2012**, *134*, 8738 – 8741.

[4] H. A. Patel, S. Hyun Je, J. Park, D. P. Chen, Y. Jung, C. T. Yavuz, A. Coskun, *Nat. Commun.* **2013**, *4*, 1357.

[5] C. D. Wood, B. Tan, A. Trewin, H. J. Niu, D. Bradshaw, M. J. Rosseinsky, Y. Z. Khimyak, N. L. Campbell, R. Kirk, E. Stockel, A. I. Cooper, *Chem. Mater.* **2007**, *19*, 2034 – 2048.

[6] a) X. Wang, K. Maeda, A. Thomas, K. Takanabe, G. Xin, J. M. Carlsson, K. Domen, M. Antonietti, *Nat. Mater.* **2009**, *8*, 76 – 80; b) R. Palkovits, M. Antonietti, P. Kuhn, A. Thomas, F. Schüth, *Angew. Chem.* **2009**, *121*, 7042 – 7045; *Angew. Chem. Int. Ed.* **2009**, *48*, 6909 – 6912; c) M. G. Schwab, B. Fassbender, H. W. Spiess, A. Thomas, X. Feng, K. Müllen, *J. Am. Chem. Soc.* **2009**, *131*, 7216 – 7217.

[7] Y. Kou, Y. Xu, Z. Guo, D. Jiang, *Angew. Chem.* **2011**, *123*, 8912 – 8916; *Angew. Chem. Int. Ed.* **2011**, *50*, 8753 – 8757.

[8] J. X. Jiang, F. Su, A. Trewin, C. D. Wood, N. L. Campbell, H. Niu, C. Dickinson, A. Y. Ganin, M. J. Rosseinsky, Y. Z. Khimyak, A. I. Cooper, *Angew. Chem.* **2007**, *119*, 8728 – 8732; *Angew. Chem. Int. Ed.* **2007**, *46*, 8574 – 8578.

[9] L. Zhang, T. Lin, X. Pan, W. Wang, T.-X. Liu, *J. Mater. Chem.* **2012**, *22*, 9861 – 9869.

[10] X. L. Feng, Y. Y. Liang, L. J. Zhi, A. Thomas, D. Q. Wu, I. Lieberwirth, U. Kolb, K. Müllen, *Adv. Funct. Mater.* **2009**, *19*, 2125 – 2129.

[11] N. Kang, J. H. Park, J. Choi, J. Jin, J. Chun, I. G. Jung, J. Jeong, J. G. Park, S. M. Lee, H. J. Kim, S. U. Son, *Angew. Chem.* **2012**, *124*, 6730 – 6734; *Angew. Chem. Int. Ed.* **2012**, *51*, 6626 – 6630.

[12] a) Z. Zuo, Y. Guo, Y. Li, J. Lv, H. Liu, J. Xu, Y. Li, *Macromol. Rapid Commun.* **2009**, *30*, 1940 – 1944; b) C. D. Wood, B. Tan, A. Trewin, F. Su, M. J. Rosseinsky, D. Bradshaw, Y. Sun, L. Zhou, A. I. Cooper, *Adv. Mater.* **2008**, *20*, 1916 – 1921.

[13] J. W. Colson, A. R. Woll, A. Mukherjee, M. P. Levendorf, E. L. Spitler, V. B. Shields, M. G. Spencer, J. Park, W. R. Dichtel, *Science* **2011**, *332*, 228 – 231.

[14] a) S. Yang, X. Feng, L. Wang, K. Tang, J. Maier, K. Müllen, *Angew. Chem.* **2010**, *122*, 4905 – 4909; *Angew. Chem. Int. Ed.* **2010**, *49*, 4795 – 4799; b) S. B. Yang, X. L. Feng, K. Müllen, *Adv. Mater.* **2011**, *23*, 3575 – 3579.

[15] a) Q. T. Qu, S. B. Yang, X. L. Feng, *Adv. Mater.* **2011**, *23*, 5574 – 5580; b) Y. Y. Liang, Y. G. Li, H. L. Wang, J. G. Zhou, J. Wang, T. Regier, H. J. Dai, *Nat. Mater.* **2011**, *10*, 780 – 786; c) H. L. Wang, L. F. Cui, Y. A. Yang, H. S. Casalongue, J. T. Robinson, Y. Y. Liang, Y. Cui, H. J. Dai, *J. Am. Chem. Soc.* **2010**, *132*, 13978 – 13980.

[16] a) H. L. Wang, Y. Y. Liang, Y. G. Li, H. J. Dai, *Angew. Chem.* **2011**, *123*, 11161 – 11164; *Angew. Chem. Int. Ed.* **2011**, *50*, 10969 – 10972; b) Y. G. Li, H. L. Wang, L. M. Xie, Y. Y. Liang, G. S. Hong, H. J. Dai, *J. Am. Chem. Soc.* **2011**, *133*, 7296 – 7299.

[17] S. B. Yang, X. L. Feng, X. C. Wang, K. Müllen, *Angew. Chem.* **2011**, *123*, 5451 – 5455; *Angew. Chem. Int. Ed.* **2011**, *50*, 5339 – 5343.

[18] Y. Su, S. Li, D. Wu, F. Zhang, H. Liang, P. Gao, C. Cheng, X. Feng, *ACS Nano* **2012**, *6*, 8349 – 8356.

[19] S. Stankovich, D. A. Dikin, G. H. B. Dommett, K. M. Kohlhaas, E. J. Zimney, E. A. Stach, R. D. Piner, S. T. Nguyen, R. S. Ruoff, *Nature* **2006**, *442*, 282 – 286.

[20] R. Chinchilla, C. Nájera, *Chem. Rev.* **2007**, *107*, 874 – 922.

[21] a) R. Dawson, A. Laybourn, Y. Z. Khimyak, D. J. Adams, A. I. Cooper, *Macromolecules* **2010**, *43*, 8524 – 8530; b) J. X. Jiang, A. Laybourn, R. Clowes, Y. Z. Khimyak, J. Bacsa, S. J. Higgins, D. J. Adams, A. I. Cooper, *Macromolecules* **2010**, *43*, 7577 – 7582.

[22] A. Pines, M. G. Gibby, J. S. Waugh, *J. Chem. Phys.* **1973**, *59*, 569 – 590.

[23] K. Schmidt-Rohr, H. W. Spiess, *Multidimensional Solid-State NMR and Polymers*, Elsevier, Amsterdam, **1994**.

[24] D. Dudenko, A. Kiersnowski, J. Shu, W. Pisula, D. Sebastiani, H. W. Spiess, M. R. Hansen, *Angew. Chem.* **2012**, *124*, 11230 – 11234; *Angew. Chem. Int. Ed.* **2012**, *51*, 11068 – 11072.

[25] N. Kobayashi, M. Kijima, *J. Mater. Chem.* **2007**, *17*, 4289 – 4296.

[26] a) Y. Zhao, K. Watanabe, K. Hashimoto, *J. Am. Chem. Soc.* **2012**, *134*, 19528 – 19531; b) M. Zhong, E. K. Kim, J. P. McGann, S.-E. Chun, J. F. Whitacre, M. Jaroniec, K. Matyjaszewski, T. Kowalewski, *J. Am. Chem. Soc.* **2012**, *134*, 14846 – 14857.

[27] J. P. Paraknowitsch, B. Wienert, Y. Zhang, A. Thomas, *Chem. Eur. J.* **2012**, *18*, 15416 – 15423.

[28] a) S. B. Yang, L. J. Zhi, K. Tang, X. L. Feng, J. Maier, K. Müllen, *Adv. Funct. Mater.* **2012**, *22*, 3634 – 3640; b) J. Liang, Y. Jiao, M. Jaroniec, S. Z. Qiao, *Angew. Chem.* **2012**, *124*, 11664 – 11668; *Angew. Chem. Int. Ed.* **2012**, *51*, 11496 – 11500.

[29] a) R. L. Liu, D. Q. Wu, X. L. Feng, K. Müllen, *Angew. Chem.* **2010**, *122*, 2619 – 2623; *Angew. Chem. Int. Ed.* **2010**, *49*, 2565 – 2569; b) S. Y. Wang, E. Iyyamperumal, A. Roy, Y. H. Xue, D. S. Yu, L. M. Dai, *Angew. Chem.* **2011**, *123*, 11960 – 11964; *Angew. Chem. Int. Ed.* **2011**, *50*, 11756 – 11760.

[30] a) Z. B. Lei, N. Christov, X. S. Zhao, *Energy Environ. Sci.* **2011**, *4*, 1866 – 1873; b) Y. W. Zhu, S. Murali, M. D. Stoller, K. J. Ganesh, W. W. Cai, P. J. Ferreira, A. Pirkle, R. M. Wallace, K. A. Cychosz, M. Thommes, D. Su, E. A. Stach, R. S. Ruoff, *Science* **2011**, *332*, 1537 – 1541; c) Z. S. Wu, Y. Sun, Y. Z. Tan, S. B. Yang, X. L. Feng, K. Müllen, *J. Am. Chem. Soc.* **2012**, *134*, 19532 – 19535; d) Z. S. Wu, A. Winter, L. Chen, Y. Sun, A. Turchanin, X. L. Feng, K. Müllen, *Adv. Mater.* **2012**, *24*, 5130 – 5135.

